Materials Science-Poland, 36(4), 2018, pp. 675-684
http://www.materialsscience.pwr.wroc.pl/
DOI: 10.2478/msp-2018-0072

sciendo

Influence of molar concentration and temperature on structural, optical, electrical and X-ray sensing properties of chemically grown nickel-bismuth-sulfide ($Ni_xBi_{2-x}S_3$) thin films

SABARISH R.[1], SURIYANARAYANAN N.[1,*], J.M. KALITA[2], M.P. SARMA[2], G. WARY[2], VIPUL KHERAJ[3], SAMPAT G. DESHMUKH[3]

[1]Department of Physics, Government College of Technology, Coimbatore-641 013, India
[2]Department of Physics, Cotton University, Guwahati-781 001, India
[3]Department of Applied Physics, Sardar Vallabhbhai National Institute of Technology, Surat-395 007, India

In this report, ternary semiconducting $Ni_xBi_{2-x}S_3$(x = 0.2 M and 0.5 M) thin films were synthesized *in situ* for the first time by a chemical bath deposition technique at different bath temperatures (60 °C, 70 °C and 80 °C). The effects of concentration and deposition temperature on the deposited films were studied by combining the results of structural, morphological, optical and electrical analyses. The growth of $Ni_xBi_{2-x}S_3$ films with good crystalline nature and interconnected grain arrangement takes place due to increasing the concentration of Ni^{2+} ions in bismuth sulfide matrix. EDS result confirmed the stoichiometry of $Ni_xBi_{2-x}S_3$ formation. Wettability test demonstrated that the surface of the film was hydrophilic in nature. The optical absorption spectra revealed that the bandgap E_g of the x = 0.5 M film deposited at 70 °C was about 1.36 eV. Current-voltage (I-V) characteristics of the x = 0.5 M film deposited at 70 °C were studied under X-ray radiation and dark condition. An X-ray detection sensitivity analysis showed that the detection sensitivity is optimum when the bias voltage applied across the film is low (∼0.9 V). These findings reveal that the film with x = 0.5 M deposited at 70 °C can be used as an efficient low cost X-ray sensor.

Keywords: *chemical bath deposition; X-ray; photoluminescence; ternary compounds; activation energy; sensor*

1. Introduction

In the past decade, investigations on ternary semiconducting thin films have significantly increased due to novel optical and electrical properties of these compounds. One of the major factors driving the current interest in the ternary semiconducting materials is their appropriateness to devices such as solar cells [1, 2], sensors [3] and supercapacitors [4]. Creation of solar energy devices and sensors using ternary semiconductor is of great interest due to their high conversion efficiency, tunable band gap energy and reliability [5]. Hence, ternary semiconducting chalcogenides have posed attention on their photonic and sensing applications.

For the preparation of ternary thin films, many researchers have used various techniques, such as spray pyrolysis [6–8], thermal deposition [9, 10], chemical vapor deposition [11, 12] and chemical bath deposition (CBD) [13–15]. Among these deposition techniques, CBD has several advantages, as it is an uncomplicated, economic and well-suited method for the deposition of semiconducting materials. It does not require highly sophisticated instruments and can easily be adapted for large area deposition. Quality of coated thin films can be simply varied by growth parameters, such as metal ion concentration, deposition time, bath temperature, substrate and complex reagent, etc. Among various ternary chalcogenides, bismuth sulfide based ternary compounds, such as $CuBiS_2$ and $PbBiS_2$, with their significant photoconductivity and sensitivity can be used as an alternative absorber layer in thin film solar cells [16, 17].

*E-mail: nsuri22@gmail.com

Bismuth sulfide is a V-VI group semiconductor with optimum band gap energy of 1.69 eV [6] that lies between visible regions of the solar energy band. Due to such band gap, it has been found to be a very useful material for the fabrication of photovoltaic devices, photoconductors, etc. [18–20]. On the other hand, nickel sulfide is a typical VIII-VI group semiconductor having a bandgap energy of 0.9 eV [21]. It is widely used for batteries [22, 23], dye-sensitized solar cells [24], supercapacitors [25], etc.

The nickel bismuth sulfide $Ni_xBi_{2-x}S_3$ ternary semiconducting compound is of current interest because of its beneficial band gap. The optical and electrical properties of binary Bi_2S_3 and NiS compounds were reported by many researchers. In contrast, there is a limited literature on the physical properties of ternary $Ni_xBi_{2-x}S_3$ compounds. Therefore, our major interest in this report is to investigate the structural, surface morphological, optical and electrical characteristics of $Ni_xBi_{2-x}S_3$ films prepared by a chemical bath deposition technique. The study is further extended by investigation of X-ray radiation sensing properties of the films.

2. Experimental

Primarily, the glass substrates (75 mm × 25 mm × 1.45 mm) were washed with a detergent solution and boiled in chromic acid for 20 min followed by washing in double distilled water. Finally, the substrates were ultrasonically cleaned using isopropyl alcohol and dried.

For the preparation of $Ni_xBi_{2-x}S_3$ thin films, AR grade nickel nitrate hexahydrate was used as a nickel ion source, bismuth nitrate pentahydrate as a bismuth ion source, and sodium thiosulfate as a sulfide ion source. The solution prepared at room temperature was mixed together and stirred continuously for 45 min. For different concentrations of nickel (x = 0.2 M and 0.5 M), separate precursor solutions were prepared. After addition of ion sources, mild yellow solution gently transformed to blackish green color while stirring. Ethylene diamine tetra acetic acid disodium salt (EDTA) was added dropwise for complex formation and obtaining uniform thin film over the substrate. Generally, EDTA acts as a complex forming agent and stabilizes ions. Formation of the complex causes controlled release of ions and helps avoid molecular segregation, which results in forming a homogenous solution [26]. The glass substrates were vertically immersed in the solution and the bath temperature was maintained at 60 °C for 3 h. Subsequently, the solution was cooled to room temperature and kept for 6 h. Finally, the deposited films were rinsed by distilled water to remove loosely bound particles from the surface. The obtained films were dark brown in color, shiny, and showed good adherence with high uniformity over the glass substrate. Using similar process, the films were prepared at 70 °C and 80 °C bath temperatures. After deposition, all the films were annealed at 500 °C to remove any existing water.

Reaction mechanism [27, 28]:

(i) Formation of metal complexes

Aqueous solution of $Bi(NO_3)_{3.5}H_2O$ with EDTA results in formation of complex species. Reaction of bismuth ions in the presence of EDTA follows the scheme:

$$Bi(NO_3)_3 \cdot 5H_2O + EDTA^{4-} \rightarrow [Bi(EDTA)]^{1-} + 5H_2O \quad (1)$$

Similarly, nickel ions with EDTA react as:

$$Ni(NO_3)_2 \cdot 6H_2O + EDTA^{4-} \rightarrow [Ni(EDTA)]^{2-} + 6H_2O \quad (2)$$

(ii) Dissociation of sodium thiosulfate

$$Na_2S_2O_3 \rightarrow 2Na^+ + S_2O_3^{2-} \quad (3)$$

In acidic medium:

$$4.5S_2O_3^{2-} + 9H^+ \rightarrow 6HSO_4^- + 3S^{2-} \quad (4)$$

(iii) The net reaction for $Ni_xBi_{2-x}S_3$ formation

$$[Bi(EDTA)]^{1-} + [Ni(EDTA)]^{2-} + 8H^+ + 3S^{2-} \rightarrow Ni_xBi_{2-x}S_3 + 2EDTA \quad (5)$$

$$[Bi(EDTA)]^{1-} + [Ni(EDTA)]^{2-} + 8H^+ + 3S^{2-} \rightarrow Ni_{0.2}Bi_{1.8}S_3 + 2EDTA \ (\text{for } x = 0.2\,M) \quad (6)$$

$$[Bi(EDTA)]^{1-} + [Ni(EDTA)]^{2-} + 8H^{+} + 3S^{2-} \rightarrow Ni_{0.5}Bi_{1.5}S_3 + 2EDTA \text{ (for } x = 0.5\ M) \quad (7)$$

The ternary films deposited under these conditions were analyzed using X-ray diffraction (XRD), scanning electron microscopy (SEM), energy dispersive X-ray spectroscopy (EDS), UV-Vis absorption spectroscopy and photoluminescence (PL). The crystalline structure was studied from the XRD patterns (Shimadzu XRD 6000), the surface morphology was studied by SEM (VEGA3), stoichiometry by EDS, optical band gap energy from absorption spectra recorded by UV-Vis spectroscopy (Agilent Cary-100), photo-optical properties by PL spectroscopy (Cary Eclipse-EL08083851) and electrical properties by Keithley electrometer (6517B).

3. Results and discussion

3.1. Structural analysis

Fig. 1 shows typical X-ray diffraction (XRD) patterns of the $Ni_xBi_{2-x}S_3$ thin films with x = 0.2 M and 0.5 M deposited at various bath temperatures (60 °C, 70 °C and 80 °C). The standard diffraction profile of nickel bismuth sulfide (JCPDS# 80-2190) is also shown for ease of reference. The XRD pattern exhibits sharp and intense diffraction peaks. It shows the crystalline nature of the deposited films. The major diffraction peaks centered at 22.30°, 32.27°, 39.35°, 51.04° and 57.03° (2θ angle) correspond to (1 1 0), (2 0 0), (2 0 1), (2 2 1) and (3 1 1) planes assigned to orthorhombic crystal phase of nickel bismuth sulfide. This indicates the formation of nickel bismuth sulfide. From Fig. 1, it can be clearly seen that the intensity of the diffraction peaks is increased with the increase in Ni concentration (0.2 M to 0.5 M) and bath temperature (60 °C to 80 °C). It indicates that the degree of crystallinity improves at higher concentration of Ni^{2+} ions in bismuth sulfide matrix. Further, the increase in intensity with bath temperature is also due to increase in reaction rate. In the XRD patterns, no secondary phases are observed. The broad diffraction peaks reveal the nanocrystalline nature of the deposited films. The average crystallite size was determined from the Debye-Scherrer formula [29]:

$$D = \frac{k\lambda}{B\cos\theta} \quad (8)$$

where D is the mean crystallite size, λ the wavelength of the X-ray used (1.54 Å), k is shape factor (0.9), B is the full width half maximum and θ is the diffraction angle. The crystallite size values are reported in Table 1.

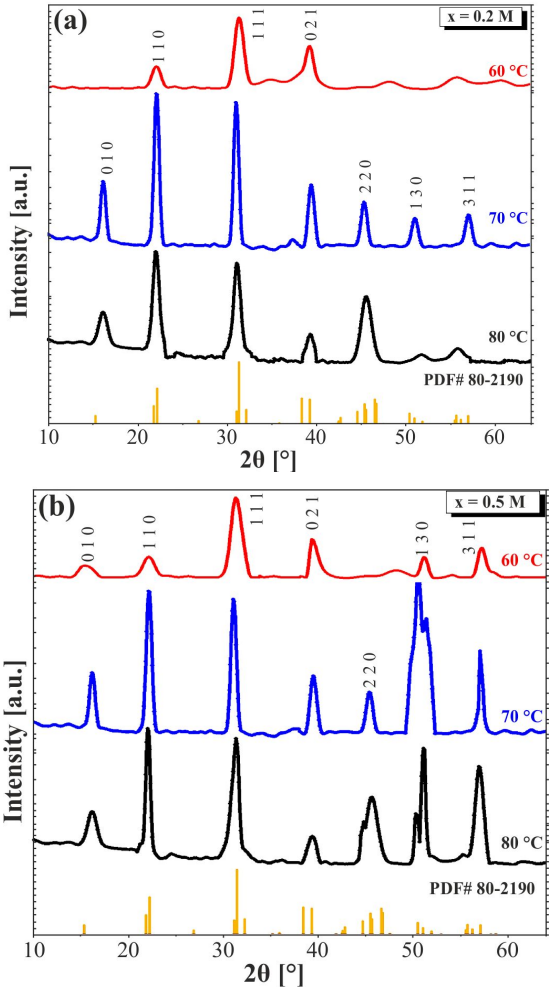

Fig. 1. XRD pattern of $Ni_xBi_{2-x}S_3$ for (a) x = 0.2 M and (b) x = 0.5 M films deposited at 60 °C, 70 °C and 80 °C.

In order to evaluate the crystallite size and to calculate the probable microstrain in the films, the W-H (Williamson-Hall) [30] analysis has been carried out. According to the Williamson-Hall model,

Table 1. Structural parameters, thickness and bandgap energy of the $Ni_xBi_{2-x}S_3$ (x = 0.2 M and 0.5 M) thin films deposited at the bath temperature of 60 °C, 70 °C and 80 °C.

Concentration	Deposition temperature [°C]	D [nm] (Debye-Scherrer method)	D [nm] (W-H method)	Microstrain ($\times 10^{-3}$)	Dislocation density [$\times 10^{16}$ lines per m^2]	Thickness [nm]	Bandgap energy [eV]
x = 0.2 M	60	15.96	12.78	3.554	6.12	186	1.77
	70	17.82	17.71	2.947	3.15	203	1.64
	80	16.33	14.77	3.234	4.58	197	1.71
x = 0.5 M	60	16.32	13.04	3.431	5.88	193	1.47
	70	18.21	18.15	2.835	3.02	215	1.36
	80	17.02	15.23	3.411	4.31	206	1.40

the broadening of a multiple ordered diffracted peak having full width at half maximum, β is related with the crystallite size, D as:

$$\beta = \frac{\lambda}{D\cos\theta} + 4\,\varepsilon\,\tan\theta \tag{9}$$

where λ is the wavelength of X-ray, θ is the diffraction angle and ϵ is the microstrain present in the crystal lattice of the films. According to equation 7, a plot of βcosθ/λ against 2sinθ/λ is linear with a slope 2ϵ and intercept equal to 1/D. The W-H plots corresponding to the films deposited at 60 °C, 70 °C and 80 °C for various concentrations (x = 0.2 M and 0.5 M) are shown in Fig. 2. The dislocation density δ is calculated from the Williamson-Smallman formula [31]:

$$\delta = \frac{n}{D^2} \tag{10}$$

where n is a constant. For minimum dislocation density, n = 1. Table 1 provides the structural data of deposited films with various concentrations and bath temperatures. Table 1 reveals that the average crystalline size D calculated using W-H method is slightly smaller than that obtained with Debye-Scherrer method. This may be caused by the effect of microstrain on the diffraction peaks. The microstrain and dislocation density were found to decrease with an increase in concentration (0.2 M to 0.5 M) and bath temperature (60 °C to 70 °C). But at the bath temperature of 80 °C, the microstrain slightly increased due to the formation of clusters which, in turn, increased the strain at high temperatures. This analysis explains why the film deposited at 70 °C for x = 0.5 M has an optimum quality.

The thickness of the $Ni_xBi_{2-x}S_3$ films was estimated by profilometry method. The values of film thickness corresponding to the films which were deposited at various concentrations and bath temperatures are reported in Table 1. This analysis shows that for both concentrations, x = 0.2 M and 0.5 M, the thickness of the film deposited at 70 °C reaches maximum and decreases with further increase of bath temperature. This may be due to random motion of the ions at high temperature which decreases the deposition rate.

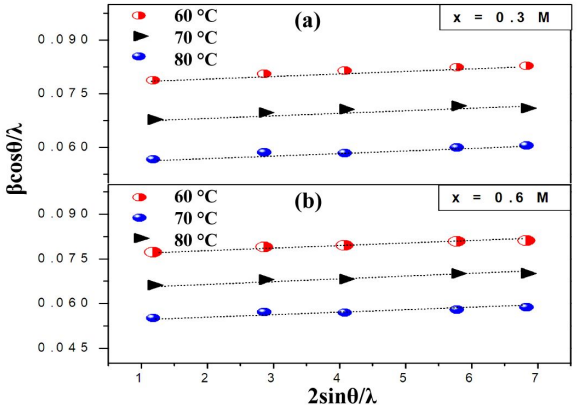

Fig. 2. W-H plot for the $Ni_xBi_{2-x}S_3$ films corresponding to (a) x = 0.2 M, (b) x = 0.5 M deposited at 60 °C, 70 °C and 80 °C.

3.2. Surface morphology and EDS

The scanning electron microscope SEM images of the $Ni_xBi_{2-x}S_3$ films corresponding to various concentrations and bath temperatures are

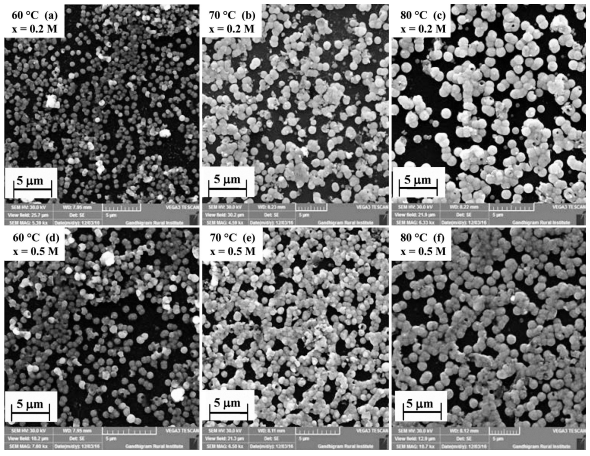

Fig. 3. SEM micrographs of the $Ni_xBi_{2-x}S_3$, x = 0.2 M films deposited at (a) 60 °C, (b) 70 °C, (c) 80 °C, and x = 0.5 M films deposited at (d) 60 °C, (e) 70 °C, (f) 80 °C.

shown in Fig. 3. The micrographs show the surface morphology of the deposited films. In the present study, both concentration and bath temperature played a significant role in deciding the reaction rate during the chemical deposition of $Ni_xBi_{2-x}S_3$. Agglomeration of grains is observed with the increase in concentration (0.2 M to 0.5 M) and bath temperature (60 °C to 80 °C). For both concentrations (0.2 M and 0.5 M) beyond the bath temperature of 60 °C, the grains are found to be spherically shaped and uniformly distributed over entire area of the substrate (Fig. 3b, Fig. 3c, Fig. 3e, Fig. 3f). However, the formation of larger grains is observed at the bath temperature of 70 °C for the compositions x = 0.2 M (Fig. 3b) and x = 0.5 M (Fig. 3e) compared to the other films. This result agrees well with the X-ray diffraction analysis. The SEM analysis shows agglomerated cluster-like grains of spherical shape with uniform distribution. The grain sizes are in the range of 170 nm to 290 nm. This analysis substantiates that the quality of the films deposited at the bath temperature of 70 °C is better than that of the other films deposited at 60 °C and 80 °C. Therefore, FE-SEM analysis was further carried out for the films deposited at 70 °C for compositions x = 0.2 M and 0.5 M (Fig. 4). This analysis clearly indicates that nanospherical grains have interfused together and distributed on the substrate. Moreover, at the concentration of x = 0.5 M (Fig. 4b) coalescence of grains is predominant compared to the films deposited at x = 0.2 M (Fig. 4a). As the film deposited at 70 °C with the composition x = 0.5 M seems to have better quality than the others, the surface morphology of the film was studied using AFM. Fig. 5a shows an AFM image of the films (x = 0.5 M) deposited at 70 °C. From the AFM analysis, the root mean square roughness [32] was estimated as 205 nm only. Further, the result of wettability studies carried out for the films (x = 0.5 M) deposited at 70 °C is shown in Fig. 5b. The wettability investigation illustrates the interaction between solid and liquid, characterized by the microscopic parameter of contact angle. From Fig. 5b, the water contact angle was found to be 57.8°, confirming that the surface is hydrophilic (water contact angle $\leqslant 10°$) in nature [17].

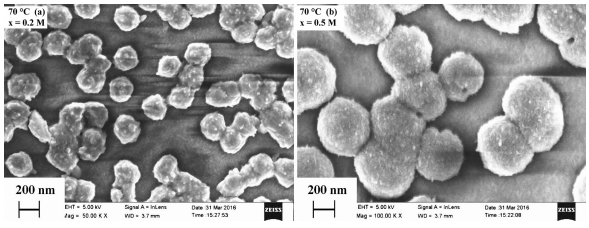

Fig. 4. FE-SEM micrographs of the $Ni_xBi_{2-x}S_3$ films corresponding to (a) x = 0.2 M, and (b) x = 0.5 M, deposited at 70 °C.

Quantitative and compositional analyses of the deposited films were carried out by EDS technique. The EDS spectra of the film deposited at 70 °C (x = 0.2 M and 0.5 M) are shown in Fig. 6. The EDS spectra clearly reveal the presence of Bi, Ni, S and Si. Inset tables (Fig. 6a and Fig. 6b) show the atomic composition percentage of the elements present in the films. The presence of silicon observed in the EDS patterns corresponds to the glass substrate. The composition is found to be homogeneous and stoichiometric. This indicates the formation of $Ni_xBi_{2-x}S_3$ thin films.

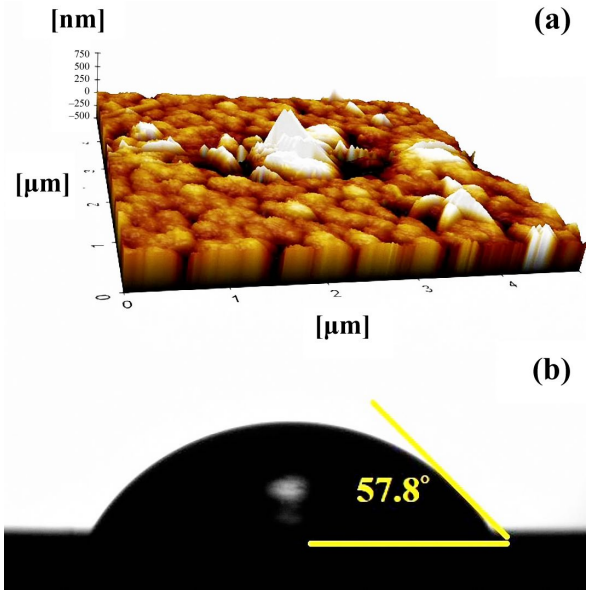

Fig. 5. (a) AFM micrograph of $Ni_xBi_{2-x}S_3$ (x = 0.5 M) film deposited at 70 °C, (b) wettability analysis of the film.

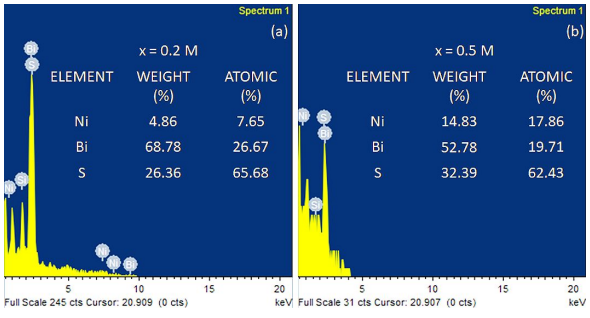

Fig. 6. EDS spectra of the $Ni_xBi_{2-x}S_3$ (a) x = 0.2 M, (b) x = 0.5 M films deposited at 70 °C.

3.3. Optical properties: UV-Vis absorption studies

Fig. 7a and Fig. 7b show the absorption spectra of $Ni_xBi_{2-x}S_3$ (x = 0.2 M and x = 0.5 M) films recorded between 200 nm and 1200 nm. It is observed that the film with x = 0.2 M has low absorbance around the UV region and visible region (Fig. 7a). It is worth noting that the absorption peak increases in the visible region for x = 0.5 M (Fig. 7b), while no appreciable change in absorption is noticed with an increase in bath temperatures. This may be caused by the increase in crystallite size as it was evidenced by the XRD patterns which evidently revealed the improvement in the crystallinity of the film with the increase in concentration of nickel (x = 0.2 to 0.5 M). Moreover, optical absorbance has also increased with an increase in film thickness. This could be explained by the fact that the thicker films contain more number of atoms and hence, more states are available for the photons to be absorbed. The bandgap energies of the films, corresponding to the energy value necessary to transform electrons from the valence band to conduction band, were calculated from the absorption spectra. The value of bandgap energy E_g can be estimated from the Tauc equation [33]:

$$(\alpha h\upsilon)^2 = A(h\upsilon - E_g)^n \tag{11}$$

where A is a constant, hυ is energy [eV] of incident photon, α is optical absorption coefficient, and the constant n = 1/2 for allowed direct band gap transitions [34–36]. Fig. 7c and Fig. 7d show the $(\alpha h\upsilon)^2$ versus energy hυ plot. After extrapolation of the linear portion of the plot, the band gap E_g of the films was estimated (Fig. 7c, Fig. 7d) and reported in Table 1. The band gap was found to depend on concentration of nickel as well as deposition temperature. For both concentrations (x = 0.2 and 0.5 M), the band gap of the films deposited at 70 °C was found to be smaller than those of the other films deposited at 60 °C or 80 °C. On the other hand, the band gap of the films corresponding to x = 0.5 M is smaller than that of the films having x = 0.2 M. These variations of band gap are due to several factors, such as concentration, bath temperature, thickness, etc. The reduction of band gap with concentration may be caused by the effect of impurity energy levels in high concentration films. Moreover, in thicker films, localized states are built-in conduction band which reduces the band gap [37–39].

3.4. Photoluminescence studies

Photoluminescence (PL) is a technique which is used to attain information about electron hole recombination, defects and oxygen vacancies. The room temperature PL spectra of the deposited

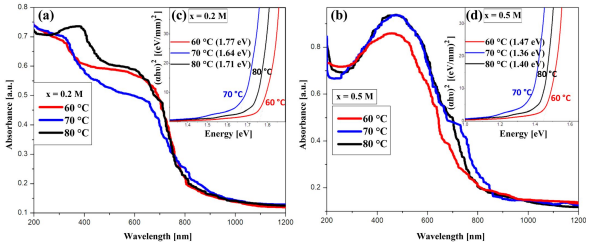

Fig. 7. Absorbance spectra of (a) x = 0.2 M, (b) x = 0.5 M films deposited at 60 °C, 70 °C, 80 °C, and plots of $(\alpha h\upsilon)^2$ versus $h\upsilon$ corresponding to the absorption spectra of (c) x = 0.2 M, (d) x = 0.5 M films deposited at 60 °C, 70 °C, 80 °C.

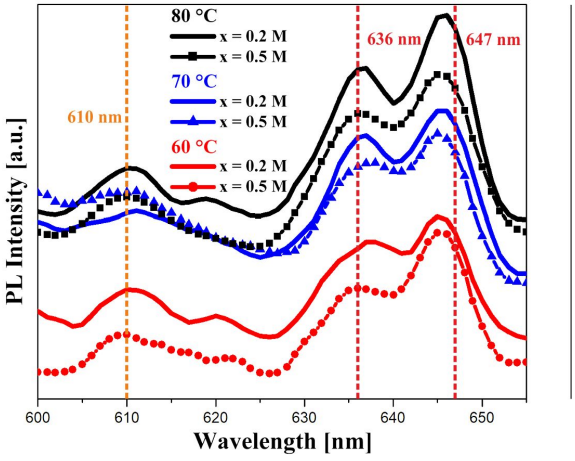

Fig. 8. Photoluminescence spectra of $Ni_xBi_{2-x}S_3$ (x = 0.2 M and x = 0.5 M) films deposited at 60 °C, 70 °C, 80 °C.

films are shown in Fig. 8. The spectra corresponding to different concentrations (x = 0.2 M and x = 0.5 M) and deposition temperatures (60 °C, 70 °C, 80 °C) are identical but they differ by their intensity. The spectra exhibit two distinct sharp emission peaks, centered at 636 nm (red band) and 647 nm (red band). The additional weak band appearing at 610 nm (orange band) may be due to the band edge luminescence of semiconducting interface. Such phenomenon of band edge luminescence, typical of ternary semiconductor is well known and extensively reported in the literature [40, 41]. The sharp peaks around 636 nm and 647 nm occur due to the presence of sulfur vacancies and stimulated centers of Ni interstitial states associated with the nanostructures of Bi. Fig. 9a shows the schematic depiction of possible emission transitions. It evidently infers the Stokes shift that is associated with the excitonic emission [40, 42]. Fig. 9b indicates the intensity variation of PL spectra in the deposited films. It shows that the increase in concentration and bath temperature increases the intensity of the PL emission. This may be due to the radiative recombination of electron and hole at localized states.

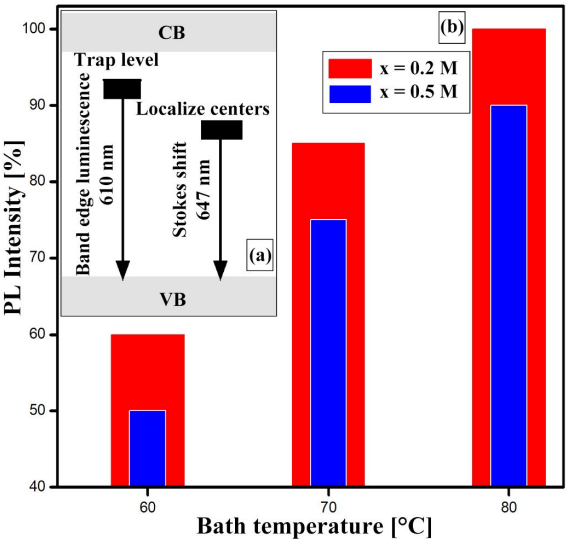

Fig. 9. (a) schematic representation of emission transitions for deposited films. (b) PL intensity versus bath temperature (60 °C, 70 °C, 80 °C) of $Ni_xBi_{2-x}S_3$ (x = 0.2 M and x = 0.5 M).

3.5. Electrical properties

The structural analyses showed that the $Ni_xBi_{2-x}S_3$ (x = 0.2 and 0.5 M) films deposited at 70 °C have larger crystallite size than the films deposited at 60 °C or 80 °C. Moreover, the dislocation density and microstrain corresponding to the film deposited at 70 °C was found to be the lowest. This implies that the films deposited at 70 °C have better lattice quality compared to the films deposited at 60 °C and 80 °C. On the other hand, the band gap of the $Ni_xBi_{2-x}S_3$ film deposited at 70 °C corresponding to x = 0.5 M is smaller than that of x = 0.2 M. Owing to smaller band gap, the conductivity of the film with x = 0.5 M can

be expected to be higher than that of the film with x = 0.2 M. Therefore, the films with x = 0.5 deposited at 70 °C have been selected to study their electrical properties from I-V characteristics. The I-V characteristics were measured under dark condition and X-ray radiation to study the influence of X-ray on the current following through the film.

Fig. 10a shows the I-V characteristics of the film recorded under dark conditions and X-ray radiation. It is evident that the current at a constant bias voltage under X-ray radiation is significantly higher than the dark current. The minimum voltage necessary to achieve the dark current ($\sim 1 \times 10^{-12}$ A) is 0.2 V, whereas under X-ray radiation, almost the same value of current is found to flow through the external circuit only at 0.04 V. The enhancement of the current under X-ray radiation has been explained on the basis of energy band model proposed by Sarma et al. [43, 44]. Under dark condition, when the voltage across the film is increased, at 0.2 V, only a few number of electrons are excited from the valence band (VB) to the conduction band (CB) to drift through the external circuit. Further increase in voltage, makes higher number of electrons to jump to the CB. Hence, the current through the external circuit increases linearly as observed in Fig. 10a. Under X-ray radiation, the number of electrons excited from VB to the CB is found to be nearly the same at just 0.04 V. This voltage is approximately one order of magnitude smaller than the minimum voltage necessary to initiate the current in dark condition. This signifies that the current contributed by the electrons under X-ray radiation is of the identical origin as that under the dark condition. The electrical conductivity under X-ray radiation and dark condition has been determined from the I-V characteristics as $\sim 2.17 \times 10^{-4}$ S/cm and $\sim 6.88 \times 10^{-6}$ S/cm, respectively.

The sensitivity of X-ray radiation as a function of applied bias voltage has been estimated using the equation:

$$S(V) = \frac{(I_r - I_d)}{I_d} \tag{12}$$

where I_r is the current under radiation and I_d is the current under dark condition [43]. In this experiment, X-ray energy was kept constant by fixing the X-ray source potential at 35 kV and filament current at 15 mA. Fig. 10b shows the variation of X-ray radiation sensitivity against applied bias voltage. It has been observed that the sensitivity decreases with the bias voltage. The analogous decrease of sensitivity with bias voltage was also found for ZnS [43] and TiO_2 [44]. When the bias voltage increases, large number of electrons are excited to the CB by the potential and only a few by the X-ray radiation. Accordingly, the current contributed by the electrons that are excited by X-ray radiation becomes lesser than that excited by the potential. Therefore, the detection sensitivity decreases with the increase in bias voltage [43, 44].

To analyze the detection sensitivity for X-ray having different energy values, the X-ray source potential was varied between 25 kV and 35 kV at a constant filament current of 15 mA. Fig. 11 shows the variation of current versus X-ray source potential for various bias-voltages, V = 0.9 V, 1.0 V, 1.5 V, 2.0 V and 3.0 V. For all bias voltages V, the current was found to increase linearly with X-ray source potential. It ensures that the current increases linearly with the energy of X-ray radiation. It clearly indicates that the current for higher bias voltage (3.0 V) is greater than for the lower bias voltage. Hence, the number of electrons excited to conduction band is larger at higher bias voltage compared to low bias voltage. The slope of the plots corresponding to bias voltages of 0.9 V, 1.0 V, 1.5 V, 2.0 V and 3.0 V, were 0.58×10^{-11}, 0.68×10^{-11}, 1.19×10^{-11}, 1.64×10^{-11}, and 1.82×10^{-11}, respectively. The slope values increase gradually with an increase in bias voltage. This is due to the current contributed by the larger number of excited electrons by high electric potential, which increases with bias voltages.

The sensitivity was calculated using I_d and I_r values measured under dark and X-ray radiation at a particular bias voltage. Fig. 12 illustrates the variation of sensitivity with X-ray source potential for different bias voltages V = 0.9 V, 1.0 V, 1.5 V, 2.0 V and 3.0 V. With a decrease in the bias voltage form 3.0 V to 0.9 V, the sensitivity is found to increase with X-ray source potential. The magnitudes

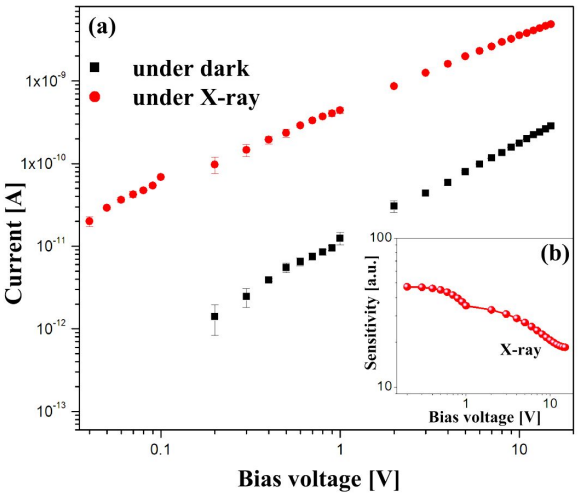

Fig. 10. (a) I-V characteristics of the $Ni_xBi_{2-x}S_3$ (x = 0.5 M) film recorded under X-ray and dark conditions; (b) variation of X-ray radiation sensitivity with bias voltage.

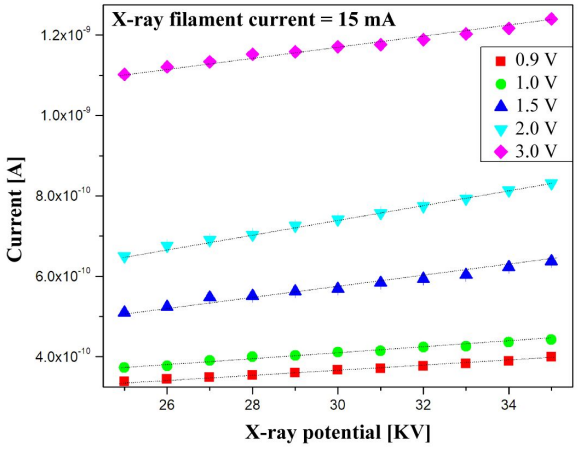

Fig. 11. Variation of current with X-ray source potential for various bias voltages V = 0.9 V, 1.0 V, 1.5 V, 2.0 V and 3.0 V.

of the slope corresponding to bias voltages 0.9 V, 1.0 V, 1.5 V, 2.0 V and 3.0 V were calculated as 0.614, 0.579, 0.552, 0.544 and 0.284, respectively. The slope value corresponding to the bias voltage of 0.9 V is the highest and it decreases gradually with an increase in bias voltage. This implies that the rate of increase in sensitivity of X-ray radiation is maximum at low bias voltage. At high bias voltage, the number of electrons excited by the applied potential exceeds the number of electrons excited by X-ray radiation. This result provides an important conclusion that the deposited $Ni_xBi_{2-x}S_3$ film is a suitable low-cost material for detection of X-ray radiation.

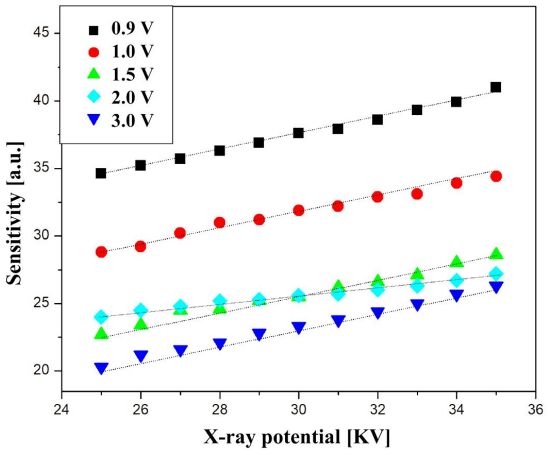

Fig. 12. Variation of sensitivity against X-ray source potential for bias voltages V = 0.9 V, 1.0 V, 1.5 V, 2.0 V, 3.0 V.

4. Conclusions

$Ni_xBi_{2-x}S_3$ thin films have been deposited on glass substrate by a chemical bath deposition technique. Effects of concentration (x = 0.2 M and 0.5 M) and bath temperature (60 °C, 70 °C, 80 °C) on structural, morphological and optical properties were investigated. The characterization results showed that the crystalline nature, surface morphology, optical and electrical properties were the best for x = 0.5 M film deposited at 70 °C. EDS analysis revealed the presence of nickel, bismuth and sulfur. Optical absorption spectrum revealed the bandgap of 1.36 eV for 0.5 M film deposited at 70 °C. PL analysis showed a strong red emission centered at 636 nm and 647 nm with high intensity for x = 0.5 M film. Further, I-V characteristics of the film were studied under X-ray and dark condition. The current under X-ray radiation was significantly greater than the current under dark condition. X-ray radiation sensitivity was found to be optimum for the bias voltage of 0.9 V. These findings demonstrate that the deposited $Ni_xBi_{2-x}S_3$ thin films can be considered as a potential optoelectronic material for X-ray radiation sensor.

References

[1] VIGIL-GALAN O., PULGARÍN F.A., CRUZ GANDARILLA F., COUREL M., VILLARREAL RUIZ G., SANCHEZ Y., JIMÉNEZ OLARTE D., SAUCEDO E., *Mater. Design*, 99 (2016), 254.

[2] YANG M., ZHANG T., SCHULZ P., LI Z., LI G., KIM D.H., GUO N., BERRY J.J., ZHU K., ZHAO Y., *Nat. Commun.*, 7 (2016), 12305.

[3] KAUR M., DADHICH B.K., SINGH R., KAILASAGANAPATHI, BAGWAIYA T., BHATTACHARYA S., DEBNATH A.K., MUTHE K.P., GADKARI S.C., *Sensor. Actuat. A-Phys.*, 242 (2017), 389.

[4] PANDIT B., SHARMA G.K., SANKAPAL B.R., *J. Colloid Interf. Sci.*, 505 (2017), 1011.

[5] LI J., KIM S.Y., NAM D., LIU X., KIM J.H., CHEONG H., LIU W., LI H., SUN Y., ZHANG Y., *Sol. Energ. Mat. Sol. C.*, 159 (2017), 447.

[6] MEDLES M., BENRAMDANE N., BOUZIDI A., NAKRELA A., TABET-DERRAZ H., KEBBAB Z., MATHIEU C., KHELIFA B., DESFEUX R., *Thin Solid Films*, 497 (2006), 58.

[7] MAHENDRAN C., SURIYANARAYANAN N., *Physica B*, 405 (2010), 2009.

[8] MAHENDRAN C., SURIYANARAYANAN N., *Physica B*, 408 (2013), 62.

[9] KANDASWAMY K., SELVIN C.P., NALINI B., ABDULLA M.I., ABHILASH K.P., *Adv. Mater. Res.*, 678 (2013), 123.

[10] REPINS I., BEALL C., VORA N., DEHART C., KUCIAUSKAS D., DIPPO P., TO B., MANN J., HSU W.C., GOODRICH A., NOUFI R., *Sol. Energ. Mat. Sol. C.*, 101 (2012), 154.

[11] DAMISA S., OLOFINJANA J., EBOMWONYI B., BAKARE O., AZI F., *Mater. Res. Express*, (2017), 2053.

[12] HAIDER A., KIZIR S., OZGIT AKGUN C., OKYAY A.K., BIYIKLI N., *J. Vac. Sci. Technol. A*, 34 (2016), 01A123.

[13] MUTHUKUMARAN S., ASHOK KUMAR M., *Mater. Lett.*, 93 (2013), 223.

[14] SOUMYA R., AJAYA K., LATA D., NARENDRA PRATAP S., MARIYA P., *J. Fluoresc.*, 26 (2015), 459.

[15] BALASUBRAMANIAN V., SURIYANARAYANAN N., PRABAHAR S., *Chalcogenide Lett.*, 8 (2011), 637.

[16] BALASUBRAMANIAN V., SURIYANARAYANAN N., *Mater. Lett.*, 91 (2013), 362.

[17] DESHMUKH S.G., PANCHAL A.K., VIPUL K., *AIP Conf. Proc.*, (2016), 20023.

[18] XUELIAN Y., CAO CHUANBAO, *Cryst. Growth Des.*, 2008 (2008), 1.

[19] MANE R.S., SANKAPAL B.R., LOKHANDE C.D., *Mater. Chem. Phys.*, 60 (1999), 158.

[20] LIU C., YANG Y., LI W., LI J., LI Y., CHEN Q., *Sci. Rep.-UK*, 6 (2016), 23451.

[21] HAMMAD A.H., ELMANDOUH Z.S., ELMELEEGI H.A., *Acta Phys. Pol. A*, 127 (2015), 901.

[22] LAI C.H., HUANG K.W., CHENG J.H., LEE C.Y., LEE W.F., HUANG C.T., HWANG B.J., CHEN L.J., *J. Mater. Chem.*, 19 (2009), 7277.

[23] WANG J., CHEW S.Y., WEXLER D., WANG G.X., NG S.H., ZHONG S., LIU H.K., *Electrochem. Commun.*, 9 (2007), 1877.

[24] ZHAO W., ZHU X., BI H., CUI H., SUN S., HUANG F., *J. Power Sources*, 242 (2013), 28.

[25] WANG A., WANG H., ZHANG S., MAO C., SONG J., NIU H., JIN B., TIAN Y., *Appl. Surf. Sci.*, 282 (2013), 704.

[26] UBALE A.U., *Mater. Chem. Phys.*, 121 (2010), 555.

[27] FAZAL T., ISMAIL B., WAFEE S., KAMBOOH A.H., KHAN A.R., *Chalcogenide Lett.*, 13 (2016), 225.

[28] ON B,P., TUBTIMTAE A., VAILIKHIT V., TEESETSOPON P., CHOOPUN S., *Phys. Lett. A*, 381 (2017), 1807.

[29] PATTERSON A.L., *Phys. Rev.*, 56 (1939), 978.

[30] WILLIAMSON G.K., HALL W.H., *Acta Metall. Sin.*, 1 (1953), 22.

[31] WILLIAMSON G.K., SMALLMAN R.E., *Philos. Mag.*, 1 (1956), 34.

[32] HORCAS I., FERNÁNDEZ R., GÓMEZ RODRÍGUEZ J.M., COLCHERO J., GÓMEZ HERRERO J., BARO A.M., *Rev. Sci. Instrum.*, 78 (2007).

[33] HE H.Y., FEI J., LU J., *Mater. Manuf. Process*, 29 (2014), 1044.

[34] SADANANDA KUMAR N., BANGERA K.V., SHIVAKUMAR G.K., *Semiconductors*, 49 (2015), 899.

[35] HUSSAIN A., BEGUM A., RAHMAN A., *Mat. Sci. Semicon. Proc.*, 21 (2014), 74.

[36] ULLAH S., MOLLAR M., MARI B., *J. Solid State Electrochem.*, (2016).

[37] TOMA O., ION L., IFTIMIE S., RADU A., ANTOHE S., *Mater. Design*, 100 (2016), 198.

[38] ATES A., YILDIRIM M.A., KUNDAKCI M., ASTAM A., *Mat. Sci. Semicon. Proc.*, 10 (2007), 281.

[39] MAN M.T., LEE H.S., *Curr. Appl. Phys.*, 15 (2015), 761.

[40] DARAFARIN S., SAHRAEI R., DANESHFAR A., *J. Alloy. Compd.*, 658 (2016), 780.

[41] SAHRAEI R., MOHAMMADI F., SOHEYLI E., ROUSHANI M., *J. Lumin.*, 187 (2017), 421.

[42] SOBHANI A., SALAVATI NIASARI M., *Superlattice. Microst.*, 59 (2013), 1.

[43] SARMA M.P., KALITA J.M., WARY G., *Mat. Sci. Semicon. Proc.*, 61 (2017), 131.

[44] SARMA M.P., KALITA J.M., WARY G., *Mater. Res. Express.*, 4 (2017), 45005.

Received 2017-11-16
Accepted 2018-07-13